Editors' Suggestion | Featured in Physics

Origin of Pulsar Radio Emission

Alexander Philippov,[1,*] Andrey Timokhin,[2] and Anatoly Spitkovsky[3]
[1]Center for Computational Astrophysics, Flatiron Institute, 162 Fifth Avenue, New York, New York 10010, USA
[2]Janusz Gil Institute of Astronomy, University of Zielona Góra, ul. Szafrana 2, 65516 Zielona Góra, Poland
[3]Department of Astrophysical Sciences, Princeton University, 4 Ivy Lane, Princeton, New Jersey 08544, USA

(Received 6 December 2019; accepted 15 April 2020; published 15 June 2020)

Since pulsars were discovered as emitters of bright coherent radio emission more than half a century ago, the cause of the emission has remained a mystery. In this Letter we demonstrate that coherent radiation can be directly generated in nonstationary pair plasma discharges which are responsible for filling the pulsar magnetosphere with plasma. By means of large-scale two-dimensional kinetic plasma simulations, we show that if pair creation is nonuniform across magnetic field lines, the screening of electric field by freshly produced pair plasma is accompanied by the emission of waves which are electromagnetic in nature. Using localized simulations of the screening process, we identify these waves as superluminal ordinary (O) modes, which should freely escape from the magnetosphere as the plasma density drops along the wave path. The spectrum of the waves is broadband and the frequency range is comparable to that of observed pulsar radio emission.

DOI: 10.1103/PhysRevLett.124.245101

Pulsars are rapidly rotating highly magnetized neutrons stars (NS), most of them are sources of coherent radio emission. It is universally accepted that active pulsars generate dense electron-positron plasma, which fills their magnetospheres. The main channel of pair creation is believed to be the absorption of γ rays in superstrong magnetic fields [1]. Pulsar radio emission has remained an enigmatic phenomenon since its discovery. Early analytical theories advocated for plasma instabilities that could be excited in the uniform pair plasma outflow above the pair formation front. The most popular ideas invoked two-stream instabilities and conversion of excited plasma waves into escaping electromagnetic radiation, or the emission of coherent curvature radiation by charge bunches [2]. The growth of two-stream instability is severely reduced by relativistic streaming of pair plasma (unless the overlap of distinct plasma clouds is invoked [3]), and it is unclear whether efficient wave conversion even happens. Theories involving charged bunches face severe difficulties of forming long-lived bunches in the first place [4]. Moreover, the last decade of kinetic plasma simulations of discharges in the pulsar magnetosphere revealed their essentially time-dependent nature, which questions any steady-state theory.

It has been demonstrated by direct numerical simulations [5,6] that electron-positron pair creation in pulsar polar caps—regions near NS magnetic poles—always proceeds via intermittent discharges. Each discharge starts with the formation of a gap—a charge-starved region with a strong electric field—where particles are accelerated to high energies until they start emitting pair-producing photons. Newly born pairs screen the accelerating electric field, thus preventing further particle acceleration. When the pair plasma leaves the polar cap, a new discharge begins. Screening of the accelerating field involves large amplitude fluctuations of the electric field and collective plasma motions. It is reasonable to expect that such screening events can produce coherent electromagnetic radiation directly [5–7].

The problem with such a straightforward mechanism is that observable electromagnetic waves should propagate in the general direction of the background magnetic field, which requires the electric field of the wave to be transverse to the background magnetic field. Excitation of such waves requires transverse charge or current fluctuations; however, in the superstrong magnetic field near polar caps charged particles can move only along the magnetic field lines. Moreover, in order to be observable, these waves have to propagate through the magnetosphere filled with dense pair plasma without substantial damping.

In this Letter, we argue that the inevitable nonuniformity of pair formation across magnetic field lines results in a fluctuating component of the electric field perpendicular to the background magnetic field and in the excitation of transverse waves. By means of first-principles kinetic plasma simulations we investigate which modes are produced in the process of a nonstationary pair plasma discharge near the NS surface. We demonstrate that the nonuniformity of pair formation across magnetic field lines leads to direct radiation of superluminal ordinary electromagnetic waves, which do not suffer from Landau damping and should be able to freely escape from the magnetosphere.

We simulate pair plasma discharge in a simplified setup in a Cartesian two-dimensional computational box. We use

a relativistic particle-in-cell code TRISTAN-MP [8]. On the left side of the box, we put a conducting plate which represents a NS, and immerse it into a background magnetic field, B_0, which is set to be along the x axis. Inside the conductor, the electric field is forced to corotation values, $E_y(y) = -(V_0 - \beta_0)B_0(y - y_0)g(y)/cR$, where y is the direction perpendicular to the background magnetic field, y_0 is the position of the conductor's center, R is its half-length, $g(y)$ is the smoothing function that drives the electric field to zero at the edge of the conductor, V_0 is the amplitude of the linear velocity of rotation, and β_0 describes the general-relativistic inertial frame-dragging effect [9]. The normal component of the magnetic field, $B_x = B_0$, is fixed at the conductor's surface. To mimic the surface charge extraction from the NS atmosphere, we inject neutral pair plasma at the boundary of the conductor. Once an electron or positron reaches the threshold energy, $\gamma_{\rm th} m_e c^2$, it begins to emit curvature photons capable of pair production. Emission and propagation of photons is done with a Monte Carlo technique, and the mean free path of photons is $R/5$. Momentum of emitted high-energy photons is directly removed from particle's momentum. To mimic spatially varying curvature of the magnetic field that determines the photon energies, we set the threshold for pair production to depend on the transverse coordinate: $\gamma_{\rm th}(y) = \gamma_0[1 + (y/R)^2]$. The simulation presented below is carried out for the following values of numerical parameters: $V_0 = 2\beta_0 = 0.2c$, $\gamma_0 = 5 \times 10^{-3}\gamma_{\rm tot} = 100$, where $\gamma_{\rm tot} = eB_0(V_0/c)(R/2)/m_e c^2$ is the Lorentz factor of a particle experiencing the full vacuum potential drop across the conducting plate. A plasma skin depth calculated for the cold plasma of a Goldreich-Julian (Ref. [18]; hereafter, GJ) density (the minimal density of plasma needed to screen the accelerating electric field in the magnetosphere of a rotating magnetized NS), $n_{\rm GJ} = V_0 B_0/4\pi cRe$, is resolved with 30 numerical cells. Though our simplified setup does not model actual physical conditions in the pulsar polar cap, the choice of numerical parameters in our experiment captures

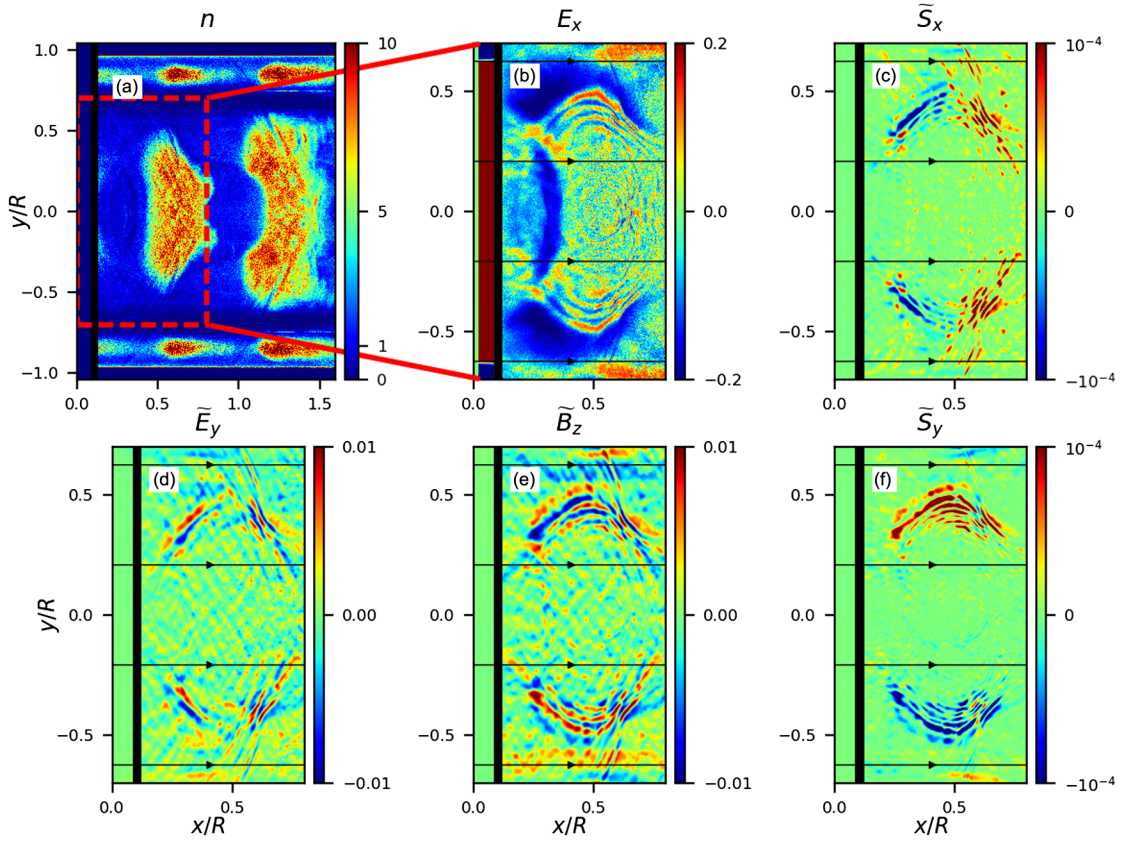

FIG. 1. Formation of the electromagnetic wave during the process of dynamic screening of the electric field in the pair plasma discharge. Individual panels show two-dimensional distributions of (a) plasma density (n), normalized to the minimum density required to carry the current, $V_0 B_0/4e\pi cR$. (b) Electric field component along the background magnetic field (E_x); electromagnetic field quantities computed by subtracting the x-averaged distributions to better visualize the wave pattern. (d) Transverse component of the electric field $\tilde{E}_y$. (c) Longitudinal component of the Poynting flux vector $\tilde{S}_x$. (e) Out-of-plane component of the magnetic field $\tilde{B}_z$. (f) Transverse component of the Poynting flux vector $\tilde{S}_y$. The electromagnetic field components are normalized to vacuum field, $(V_0/c)B_0$, and Poynting flux components are normalized to the bulk Poynting flux, $S_0 = c(V_0/c)^2 B_0^2/4\pi$, that a sheared conductor launches. In all panels distances are measured in units of the conductor's half-length, R.

the physics of particle acceleration, pair production, and dynamics of the electromagnetic fields in the polar cap accelerator [9].

Simulation starts in vacuum, and after few light crossing times along the conductor R/c it reaches a quasisteady state of repeating pair plasma production episodes followed by quiet states. In Fig. 1(a) we show a representative snapshot of plasma density produced in the simulation, which shows two pair plasma clouds produced in subsequent discharge episodes. The gap appears close to the surface of the plate. Previous episode of pair formation resulted in the plasma cloud located at $x \approx 1.2$, and we focus on the cloud located at $x \approx 0.5$. The screening of the accelerating electric field proceeds in the form of parallel electric field fluctuations clearly visible in Fig. 1(b). The nonuniformity of pair formation in the transverse (y) direction results in inhomogeneity of the electric field across magnetic field lines, i.e., in a nonzero $\nabla_y \times E_x$. This directly leads to the production of an out-of-plane fluctuating component of the magnetic field B_z. The inhomogeneity of the pair formation along the magnetic field leads to a nonuniform B_z, i.e., to a nonzero $\nabla_x \times B_z$, which gives rise to a wave component E_y (see Ref. [9] for the details of the mechanism generating transverse fields). The presence of transverse fluctuating components $\tilde{E}_y$ and $\tilde{B}_z$, clearly visible in Figs. 1(d),1(e) in regions where the pair formation front is inclined to the magnetic field, strongly suggests the electromagnetic nature of the wave. Here, $\tilde{B}_z$ and $\tilde{E}_y$ are computed as $\tilde{B}_z = B_z - \langle B_z \rangle_x$, where $\langle\rangle_x$ represents spatial averaging along the x direction and is performed to subtract the zero-frequency out-of-plane component of the magnetic field created by the bulk plasma current. The waves are linearly polarized, and their transverse electric field vector lies in the $\boldsymbol{k}$-$\boldsymbol{B}$ plane (here, $\boldsymbol{k}$ is the wave vector of propagating waves, directed at a nonzero angle with respect to the external magnetic field). This suggests that an ordinary mode is excited in the process of screening the electric field. Electric field fluctuations are accompanied by a significant transverse magnetic field component and Poynting flux only if pair production front is inclined to the local magnetic field. For example, in panels (c) and (f) of Fig. 1 the wave Poynting flux, computed as $\tilde{\mathbf{S}} = \mathbf{S} - \langle \mathbf{S} \rangle_x$, is nearly zero in the middle of the pair cloud, $y \approx 0$, where screening happens almost perpendicular to the background magnetic field direction. However, at $y/R \approx \pm 0.5$, where the screening happens at a nonzero angle to the magnetic field, the wave flux reaches $\approx 10^{-4} S_0$, where $S_0 = c(V_0/c)^2 B_0^2/4\pi$ is the bulk Poynting flux that a sheared plate launches. Interestingly, comparable wave power is emitted in both forward and backward directions. The waves that are emitted towards the NS are later reflected from the stellar surface and also propagate outwards. The discharge and wave emission repeat after most of the freshly produced pair plasma escapes from the gap region, and the accelerating electric field is restored. The timescale of this variability is slightly longer than the gap's light-crossing time.

To better understand the properties of these electromagnetic waves, we perform local 2D simulations of electric field screening during the burst of pair formation (as observed in our simulations described above) in a controlled setup, which can be considered as a zoom-in on pair formation fronts seen in Fig. 1. In this experiment, we start with a constant electric field E_0 along the background magnetic field, both pointed along the x axis. We then inject pair plasma at a constant rate $\dot{n}$ in a slab [see Fig. 2(a)], which moves at $0.999c$ along the x axis. The normal of the slab is inclined to the background magnetic field by angle α, which we vary. Pairs are injected moving with Lorentz factor $\gamma = 4$ along the direction of magnetic field. The screening of the electric field happens in two stages. Initially, freshly injected electrons and positrons are quickly accelerated by the vacuum electric field in the opposite directions, which creates a strong current $\approx 2 n_e e c = 2\dot{n} e c t$, where n_e is the local electron density. This current increases as the density of pair plasma increases, and leads to the quick screening of the electric field in time $\tau \approx \sqrt{E_0/(4\pi \dot{n} e)}$. At some point the electric field gets sufficiently low and cannot reverse the direction of motion of freshly injected pairs. After this happens, the electric field starts to oscillate, with an amplitude that slowly decreases as the plasma density increases. As more charges are available to screen the electric field, less charge separation is required for screening, and the wavelength of the oscillation decreases. The snapshots of parallel electric field component E_x and of transverse magnetic field component B_z are shown in panels (b) and (c) of Fig. 2, respectively. By performing simulations for different values of the angle α, we confirm that the amplitude of the out-of-plane component of the magnetic field in the wave scales as $B_z \approx (k_\perp/k_\parallel) E_x = E_x \sin\alpha$. In panels (d)–(f) of Fig. 2 we show horizontal slices of plasma density, electric and magnetic field components along the center of the box. We plot three vertical lines that move with the speed of light in the direction of the injected plasma. The wavefront clearly overruns the position of the lines, which suggests that the phase speed of the wave exceeds the speed of light, i.e., the excited mode is superluminal. These two facts, polarization and superluminal character, lead us to the conclusion that the wave that gets excited in the process of the discharge is an electromagnetic O mode of highly magnetized pair plasma [19]. We also find that the shape of the time series of the out-of-plane component of the magnetic field in the wave is essentially controlled by the behavior of the parallel electric field, or, by the dynamics of the discharge.

To test that the proposed mechanism can generate plasma waves with wavelengths comparable with those of pulsar radio emission we perform high resolution discharge

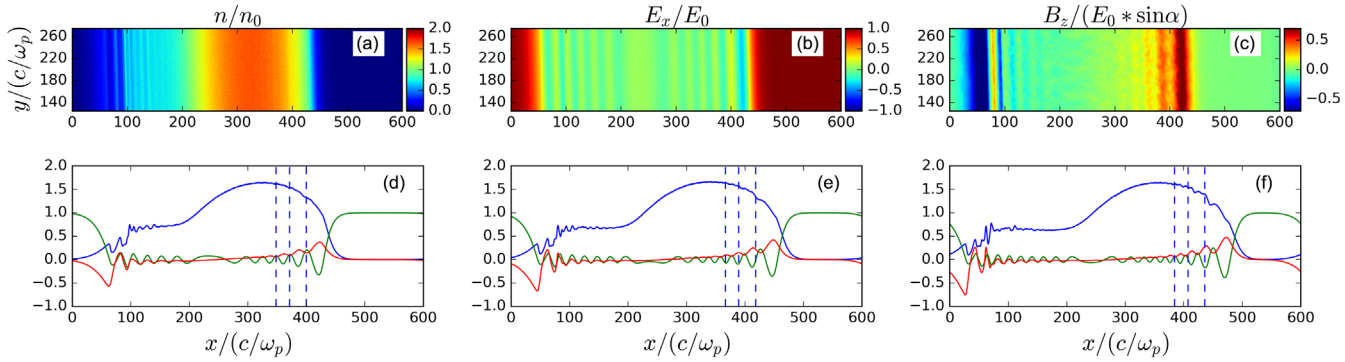

FIG. 2. Formation of the superluminal electromagnetic wave during the process of dynamic screening of the electric field. First row shows two-dimensional distributions of (a) plasma density (n). (b) Electric field component along the background magnetic field (E_x). (c) Out-of-plane component of the magnetic field (B_z), at $0.47L_x/c$, where L_x is the size of the computational box in the x direction. Panels (d)–(f) show the snapshots of n (blue line), E_x (green line), and B_z (red line) at three consecutive moments of time in the simulation, $0.47L_x/c$, $0.53L_x/c$, and $0.6L_x/c$. Blue vertical dashed lines move to the right at the speed of light. The wavefront clearly overruns the position of the lines, which proves the superluminal phase speed of the mode. Panels (a)–(c) show close-up onto the central part of our numerical domain which is larger in the y direction. Simulation is performed for the angle between the normal to plasma injection front and the background magnetic field $\alpha = 1/40$. In all panels distances are measured in units of the plasma skin depth c/ω_p, where plasma frequency $\omega_p = \sqrt{4\pi e^2 n_0/m_e}$ is calculated for the cold plasma of a fiducial density n_0.

simulations for unscaled physical parameters. We use the 1D hybrid PIC-Monte-Carlo code PAMINA [5,6] which models polar cap discharges for realistic values of all physical parameters (see Ref. [9] for the details of the numerical setup). A snapshot from these simulations is shown in Fig. 3, with values of physical parameters listed in the caption. We show the charge densities of positrons and electrons $n_\pm$, the electric field E, and the power spectrum of the electric field E_k^2 for the region where the outgoing wave is formed, shown by the gray bar in the plot for E. The emerging wave occupies a broad range of spatial frequencies visible as large amplitude fluctuations superimposed on the power-law-like part of the spectrum. Both spatial and energy distributions of newly created pair plasma are highly inhomogeneous, and the plasma frequency $\omega_p = \sqrt{4\pi e^2\langle n/\gamma^3\rangle/m_e}$ varies by a few orders of magnitude. The range of k corresponding to the range of skin depths, $\lambda_D = c/\omega_p$, in the region where the wave is forming is shown with the orange bar. The wave spectrum already spans an order of magnitude, with the shortest wavelengths reaching λ_D (not surprisingly, as the latter is the characteristic scale for the screening of the electric field). As the pair formation continues, λ_D decreases and the range of wavelengths of the plasma wave increases. Hence, the emergent coherent radiation, when it decouples from the plasma, will be broadband, extending up to the plasma frequency of pair plasma at the point of decoupling. The superluminal wave is generated by continuous pair injection, permitting the screening of the electric field on shorter and shorter scales. When the pair formation stops, so should the wave generation. The highest frequency of coherent radiation produced by this mechanism can be estimated as $\nu \simeq \sqrt{4\pi e^2 \kappa n_{\rm GJ}/\langle\gamma^3\rangle m_e}/2\pi = 26\sqrt{\kappa_5 B_{12}/r^3 P_{0.1}\gamma_{10}^3}$ GHz,

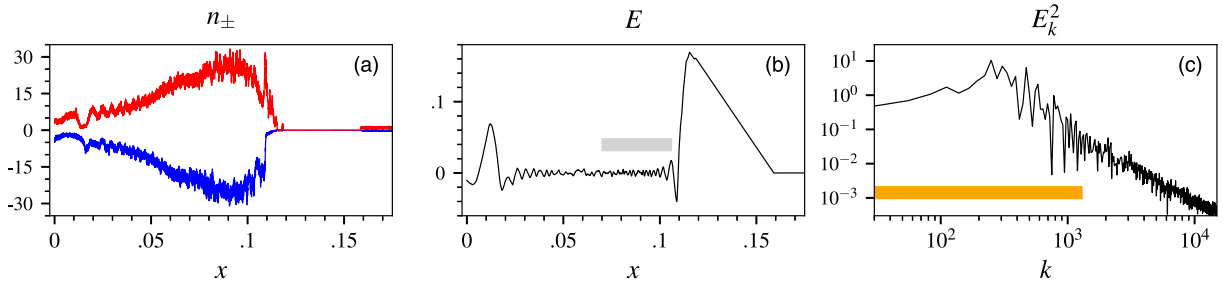

FIG. 3. One-dimensional pair discharge for realistic parameters ($P = 33$ ms, $B = 10^{12}$ G, magnetic field line radius of curvature $\rho_c = 1.67 \times 10^7$ cm). Shown are (a): charge densities $n_\pm$ of positrons (red line) and electrons (blue line), normalized to $n_{\rm GJ}$; (b) electric field E normalized to the vacuum field $E_{\rm vac} = \Omega B r_{pc}/2c = 7.6 \times 10^{10}$ V/cm; and (c) power spectrum of the electric field E_k^2 for spatial intervals shown by the gray bar in panel (b). The orange bar in panel (c) indicates the range of spatial frequencies k, measured in units of $1/L$, where $L = 0.25 r_{pc}$ is the size of the simulation box, corresponding to the range of plasma skin depths in the region shown by the gray bar in panel (b). Distance x from the NS is normalized to the polar cap radius $r_{pc} = 7.97 \times 10^4$ cm.

where κ_5 is the final pair multiplicity normalized to 10^5, $B_{12} = B/10^{12}$ G, $P_{0.1} = P/0.1$ s, r—distance from the NS in NS radii, and $\gamma_{10} = \gamma/10$ is the Lorentz factor of final pair generation. The highest pair multiplicity is usually achieved at the last cascade generation, at distances from the NS comparable to NS radius [20].

To summarize, by means of first-principles kinetic plasma simulations we presented a robust pulsar radio emission mechanism—this mechanism does not require any special physical conditions in pulsar polar caps, it should always work if pair discharges are intermittent and nonuniform across the magnetic field. These two conditions are expected to be fulfilled in polar caps of all pulsars (e.g., Refs. [6,21]). We found that if the pair formation front is inclined to the background magnetic field, the nonsteady plasma discharge produces broad-band emission in the form of the electromagnetic O mode with a spectrum controlled by the dynamics of the discharge. In pulsars, the pair formation front is inclined to the magnetic field due to, e.g., transverse variation of magnetic field line curvature or the variation of the accelerating electric field. This makes the regions near polar cap edges (where the accelerating electric field sharply jumps at the return current layer) and near magnetic poles (where the radius of curvature of magnetic field lines rapidly approaches infinity) the most efficient generators of radio emission, which might explain the existence of cone and core components in pulsar radio profiles [22].

This mechanism significantly differs from the usually postulated *ad hoc* models that require either the conversion of plasma modes from the two-stream instability or the curvature radiation from charged bunches. In fact, neither 1D nor 2D simulations of nonstationary discharge show the formation of charge density clumps or signs of streaming instabilities. It is the intrinsically time-dependent nature of plasma discharge that drives coherent radio emission [5–7]. While we find robust excitation of O modes, pulsar radio polarimetry observations suggest the presence of both O and X modes. We suggest the following mechanism that can contribute to the production of the X mode. At some distance from the star, the O mode produced in the discharge process can escape from the dense plasma cloud into a rarefied zone, where its polarization characteristics freeze. As it propagates away, the wave may encounter a dense plasma with a local magnetic field different from that where it was emitted. There the mode is no longer an eigenmode of the plasma, and may experience conversion into other plasma modes, in particular into an X mode.

The authors would like to thank J. Arons, A. Beloborodov, V. Beskin, A. Jessner, and Yu. Lyubarsky for numerous insightful discussions. A. P. and A. S. acknowledge hospitality of KITP, where part of this work was performed. This work was supported by NASA Grant No. 80NSSC18K1099 and by the National Science Foundation under Grants No. NSF AST-1616632 and No. NSF PHY-1748958. Resources supporting this work were provided by the NASA High-End Computing Program through the NASA Advanced Supercomputing Division at Ames Research Center. Research at the Flatiron Institute is supported by the Simons Foundation, which also supported A. S. (Grant No. 267233). We also thank the anonymous referees for valuable comments on the Letter.

*sphilippov@flatironinstitute.org

[1] P. A. Sturrock, Astrophys. J. **164**, 529 (1971).
[2] M. A. Ruderman and P. G. Sutherland, Astrophys. J. **196**, 51 (1975).
[3] V. V. Usov, Astrophys. J. **320**, 333 (1987).
[4] D. B. Melrose, Rev. Mod. Plasma Phys. **1**, 5 (2017).
[5] A. N. Timokhin, Mon. Not. R. Astron. Soc. **408**, 2092 (2010).
[6] A. N. Timokhin and J. Arons, Mon. Not. R. Astron. Soc. **429**, 20 (2013).
[7] A. M. Beloborodov, Astrophys. J. **683**, L41 (2008).
[8] A. Spitkovsky, Astrophysical Sources of High Energy Particles and Radiation, (2005), p. 345, https://ui.adsabs.harvard.edu/abs/2005AIPC..801..345S/abstract.
[9] See Supplemental Material at http://link.aps.org/supplemental/10.1103/PhysRevLett.124.245101 for the discussion of waves in pair plasma around pulsars and additional details about the proposed emission mechanism, numerical methods, and simulation setups, which includes Refs. [10–17].
[10] V. S. Beskin, A. V. Gurevich, and Y. N. Istomin Physics of the Pulsar Magnetosphere, (Cambridge University Press, Cambridge, 1993).
[11] A. G. Mikhaylenko, V. S. Beskin, and Y. N. Istomin, arXiv:1912.03731.
[12] A. N. Timokhin, Mon. Not. R. Astron. Soc. **368**, 1055 (2006).
[13] V. S. Beskin, Sov. Astron. Lett. **16**, 286 (1990), https://ui.adsabs.harvard.edu/abs/1990SvAL...16..286B/abstract.
[14] A. A. Philippov, B. Cerutti, A. Tchekhovskoy, and A. Spitkovsky, Astrophys. J. **815**, L19 (2015).
[15] A. A. Philippov and A. Spitkovsky, Astrophys. J. **855**, 94 (2018).
[16] M. Z. Rafat, D. B. Melrose, and A. Mastrano, J. Plasma Phys. **85**, 905850305 (2019).
[17] L. Mestel, J. A. Robertson, Y.-M. Wang, and K. C. Westfold, Mon. Not. R. Astron. Soc. **217**, 443 (1985).
[18] P. Goldreich and W. H. Julian, Astrophys. J. **157**, 869 (1969).
[19] J. Arons and J. J. Barnard, Astrophys. J. **302**, 120 (1986).
[20] A. N. Timokhin and A. K. Harding, Astrophys. J. **871**, 12 (2019).
[21] J. Arons, Astrophys. J. **266**, 215 (1983).
[22] J. M. Rankin, Astrophys. J. **352**, 247 (1990).